Pis'ma v ZhETF, vol. 96, iss. 1, pp. 59 – 63

LDA+DMFT study of magnetic transition and metallization in CoO under pressure

A. A. Dyachenko[+], *A. O. Shorikov*[+*], *A. V. Lukoyanov*[+*], *V. I. Anisimov*[+*]

[+] *Institute of Metal Physics UB RAS, 620990 Ekaterinburg, Russia*

[*] *Ural Federal University, 620002 Ekaterinburg, Russia*

Submitted 31 May 2012

In this work we report results of magnetic and spectral properties calculation for paramagnetic phase of CoO at ambient and high pressures performed within the LDA+DMFT method combining local density approximation (LDA) with dynamical mean-field theory (DMFT). From our results CoO at ambient pressure is a charge transfer insulator in the high-spin $t_{2g}^5 e_g^2$ configuration. The energy gap is continuously decreased, and finally a transition into metallic state occurs with the increase of pressure that is consistent with experimental behavior of electrical resistivity. Notably, the metal-insulator transition in CoO is found to be accompanied by the high-spin to low-spin (HS–LS) transition in agreement with XES data. The metal-insulator transition is orbital selective in the t_{2g} states of cobalt only, whereas the e_g states become metallic after the spin transition at higher pressures.

1. Introduction. For many years one of the central issues of condensed matter physics is metal-insulator transition (MIT) in *d*- or *f*-elements compounds [1]. The most spectacular examples are pressure-driven transitions from wide gap Mott insulator to metallic state in transition metal oxides. In MnO [2] and Fe_2O_3 [3] (d^5 configuration) metal-insulator transition is accompanied by high-spin to low-spin transition (HS–LS), whereas in FeO (d^6 configuration) no magnetic transition was found [4]. Recently, MIT in these materials was successfully described theoretically by the LDA+DMFT method [5] combining local density approximation (LDA) with dynamical mean-field theory (DMFT).

Cobalt monooxide also exhibits MIT under high pressure. Transport measurements at room temperature revealed that electrical resistivity in CoO shows a significant drop (about eight orders of magnitude) between 43 and 63 GPa [6]. XES measurements showed that CoO undergoes magnetic transition with the increase of pressure: when pressure grows up from ambient one the HS state is found up to 140 GPa, however, under decreasing pressure the system transits into the LS state remaining to about 97 GPa, then it reverts to HS [7].

At ambient pressure (AP) and room temperature CoO has a cubic rocksalt B1 structure which is distorted tetragonally with a slight superimposed rhombohedral distortion [8, 9] approximately at and below the Neel temperature $T_N = 289\,K$ with antiferromagnetic ordering of type II. However, at higher hydrostatic pressure at room-temperature this cubic crystal structure is transformed into rhombohedral I structure at 43 GPa, rhombohedral II at 90 GPa, and finally into the same cubic structure above 120 GPa [10, 11].

Electronic structure calculations by standard local density approximations of density functional theory (DFT) predicted an antiferromagnetic metallic ground state in CoO [12] in contrast to experimentally observed insulator with an optical band gap of $2.5 \pm 0.3\,eV$ [13]. The reason of this failure is that LSDA and GGA approaches neglect strong electron correlations in *d*-shell of transition metal, thus making impossible to reproduce experimentally observed insulator ground state at low pressures [14].

Taking into account electron correlations in the Co-3*d* states, the LDA+U method results in an insulating ground state in CoO at ambient pressure [15]. Another investigations by the LSDA+U method reproduced a magnetic transition into the LS $t_{2g}^6 e_g^1$ state, at the same time concluding that LSDA+U is inable to correctly predict the insulator-to-metal transition in this compound [16].

In similar oxide compounds, MIT and spin transitions with pressure can be successfully described within the LDA+DMFT method [2–4]. In this work we demonstrate that in our LDA+DMFT calculations both MIT and HS–LS transitions in CoO with pressure are found in very good agreement with available experimental data.

2. Method. In general, the LDA+DMFT method comprises LDA results and, on top of that, accounting for dynamical electron correlations in transition metal partially filled shells. Its computational scheme [5] is started from a non-interacting Hamiltonian $\hat{H}_{\mathrm{LDA}}$ from

a self-consistent LDA or GGA calculation, then a many-body Hamiltonian is set up, and finally the corresponding self-consistent DMFT equations are solved.

In the present work, first, *ab initio* calculations of electronic structure were obtained within the pseudopotential plane-wave method PWSCF, as implemented in the Quantum ESPRESSO package [17]. All calculation were performed for NaCl (B1) cubic crystal structure of CoO with lattice constant scaled to give a volume corresponding to applied pressure up to 140 GPa following experimental volume data [11, 18]. In the rock-salt structure of CoO the Co-d band is split by crystal field of oxygen octahedra into t_{2g} and e_g subbands, corresponding LDA partial densities of states at AP are shown in Fig. 1.

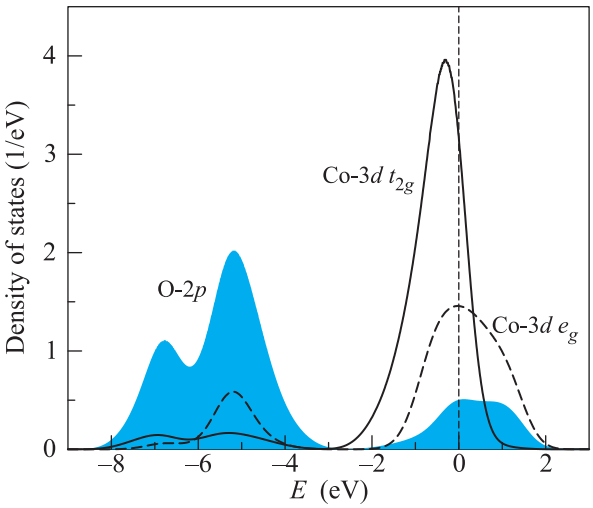

Fig. 1. Partial Co-3d and O-2p densities of states of CoO at ambient pressure from the LDA calculation

Then Hamiltonians $\hat{H}_{\mathrm{LDA}}$ in Wannier function basis [19, 20] were constructed using the projection procedure described in detail in [21]. In the basis set all bands formed by the O-2p and Co-3d states were included and, correspondingly, a full set of the O-2p, and Co-3d atomic orbitals was projected on Bloch functions for these bands.

The resulting 8×8 $p-d$ Hamiltonian to be solved by DMFT has the form

$$\hat{H} = \hat{H}_{\mathrm{LDA}} - \hat{H}_{dc} + \frac{1}{2}\sum_{i,\alpha,\beta,\sigma,\sigma'} U^{\sigma\sigma'}_{\alpha\beta}\hat{n}^{d}_{i\alpha\sigma}\hat{n}^{d}_{i\beta\sigma'}, \qquad (1)$$

where $U^{\sigma\sigma'}_{\alpha\beta}$ is the Coulomb interaction matrix, $\hat{n}^{d}_{i\alpha\sigma}$ is the occupation number operator for the d electrons with orbitals α or β and spin indices σ or σ' on the i-th site. The term $\hat{H}_{dc}$ stands for the d-d interaction already accounted for in LDA, so called double-counting correction. In the present calculation the double-counting was chosen in the following form $\hat{H}_{dc} = \bar{U}(n_{\mathrm{dmft}} - 1/2)\hat{I}$. Here, n_{dmft} is the self-consistent total number of d electrons obtained within the LDA+DMFT, $\bar{U}$ is the average Coulomb parameter for the d-shell and $\hat{I}$ is unit operator.

The elements of $U^{\sigma\sigma'}_{\alpha\beta}$ matrix were parametrized by U and J_H according to procedure described in [22]. The values of Coulomb repulsion parameter U and Hund exchange parameter J_H were calculated by the constrained LDA method [23] on Wannier functions [21]. The obtained values $J_H = 1.0\,\mathrm{eV}$ and $U = 6.0\,\mathrm{eV}$ are close to the previous estimations [16]. The effective impurity problem for the DMFT was solved by the hybridization expansion Continuous–Time Quantum Monte-Carlo method (CT–QMC) [24]. Calculations for all volumes were performed in the paramagnetic state at the inverse temperature $\beta = 1/T = 10\,\mathrm{eV}^{-1}$ corresponding to 1160 K which is well above the Neel temperature 289 K. Spectral functions on real energies were calculated from Green functions $G(\tau)$ by Maximum Entropy Method (MEM) [25].

3. Results and discussion. The LDA+DMFT calculations for CoO result in a wide gap charge transfer insulator at ambient pressure, see Fig. 2. The calculated

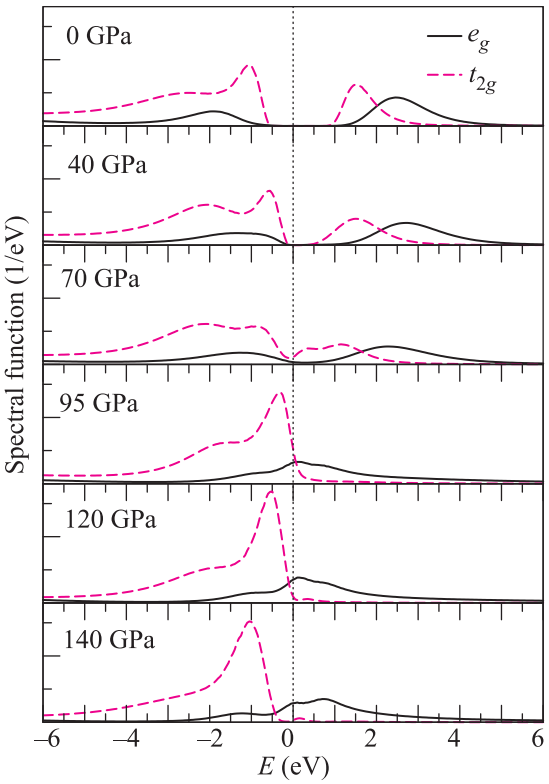

Fig. 2. Spectral functions of the t_{2g} (dashed line) and e_g (solid line) Co-3d states versus pressure obtained in the LDA+DMFT calculations

value of the energy gap about 2 eV is close to the experimental value 2.5±0.3 eV [13]. Figures 3 and 4 contain

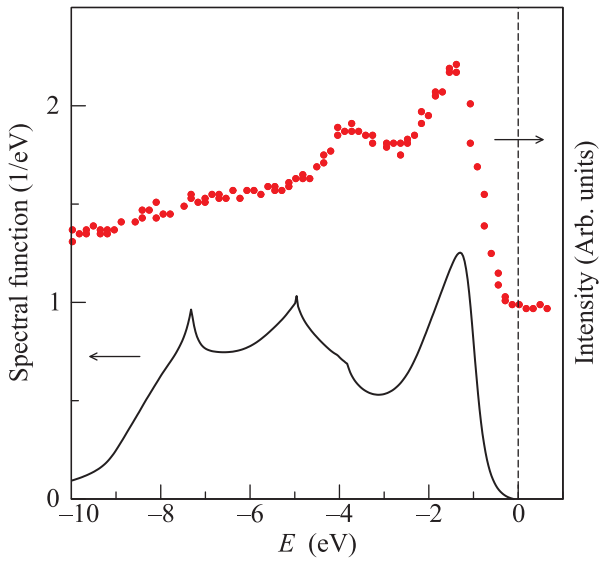

Fig. 3. Total spectral function of CoO at ambient pressure calculated within LDA+DMFT (solid line) in comparison with XPS experimental data (dots) from [13]

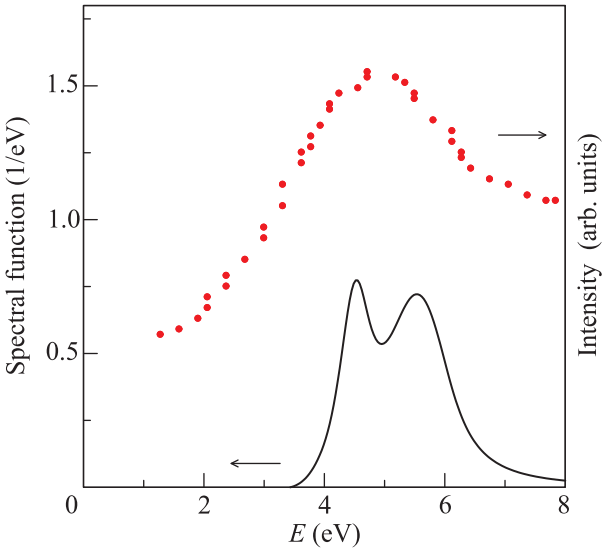

Fig. 4. Total spectral function of CoO at ambient pressure calculated within LDA+DMFT (solid line) in comparison with BIS experimental data (dots) from [13]

calculated total spectral function (including the O-2p states) compared with experimental x-ray photoemission spectroscopy (XPS) and bremsstrahlung isochromat spectroscopy (BIS) data [13]. The theoretical and experimental curves are in good agreement considering uncertainties of the Fermi level in BIS measurements.

Due to the oxygen octahedron crystal field of the Co-3d states are splitted into threefold t_{2g} and twofold e_g degenerate states. From LDA+DMFT occupation numbers are $n(e_g) = 0.55$ and $n(t_{2g}) = 0.83$ at ambient pressure. The average value of local magnetic moment $\sqrt{\langle\mu_z^2\rangle}$ is $2.81\,\mu_B$. These values agree very well with high-spin state of Co^{+2} ion (d^7 configuration) in cubic crystal field: 2 electrons occupying the e_g states and 5 electrons – the t_{2g} states with ionic magnetic moment value $3\,\mu_B$. This spin state will be changed with pressure.

The calculated spectral functions ($A(\omega)$) for all pressure values are presented in Fig. 2. Note that the spectral functions at ambient pressure phase have well defined insulating behavior for all d-orbitals. However, the energy gap for the e_g states is nearly 1.5 times larger than for the t_{2g} states indicating that they are closer to MIT. Up to 40 GPa the gap in the t_{2g} states shrinks, and it vanishes at 70 GPa, whereas the spectral function for the e_g states still has a gap of 0.5 eV at 70 GPa, see Fig. 2. Such a transition with strong orbital dependence can be classified as orbital selective Mott transition (OSMT) [26]. From the above analysis of our LDA+DMFT calculations the metallization in CoO occurs in the range 40–70 GPa that corresponds to a significant drop of eight orders of magnitude in electrical resistivity experimentally measured between 43 and 63 GPa [6].

Our LDA+DMFT results also reveal that MIT in CoO under pressure is accompanied by the change of occupation numbers of the t_{2g} and e_g cobalt states and a magnetic moment drop as it clearly follows from Fig. 5. The magnetic moment value decreases from $2.63\,\mu_B$ at

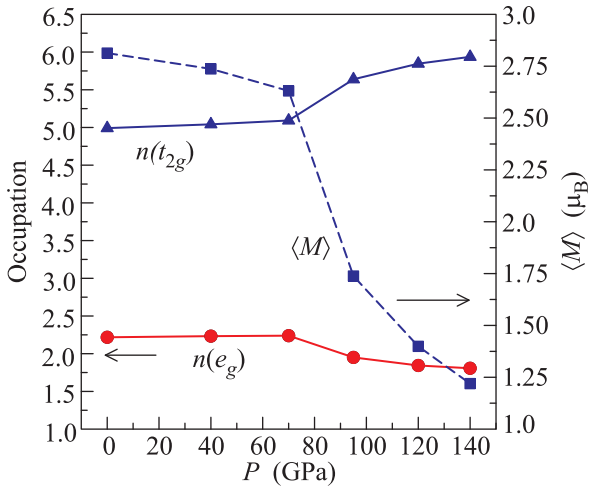

Fig. 5. Magnetic moments (squares) and occupancies of t_{2g} (triangles) and e_g (circles) shells versus pressure obtained in the LDA+DMFT calculations

70 GPa to 1.73 μ_B at 95 GPa and 1.21 μ_B at 140 GPa. At high pressure occupation numbers become $n(e_g) = 0.45$, $n(t_{2g}) = 0.99$ at 140 GPa that corresponds to the LS $t_{2g}^6 e_g^1$ state. Thus the HS–LS $t_{2g}^5 e_g^2 \rightarrow t_{2g}^6 e_g^1$ transition in CoO is clearly manifested in this significant drop of magnetic moment that starts from 70 GPa together with redistribution of the orbital occupation numbers to the low-spin configuration. The obtained results agrees well with experimental XES data evidencing for the clear LS state below 97 GPa and the HS–LS transition region where both HS and LS states can be found from 97 to 140 GPa [7].

To clarify the electronic configuration of CoO at high pressure, we also performed calculations of atomic state weights from our LDA+DMFT results, see Fig. 6. These

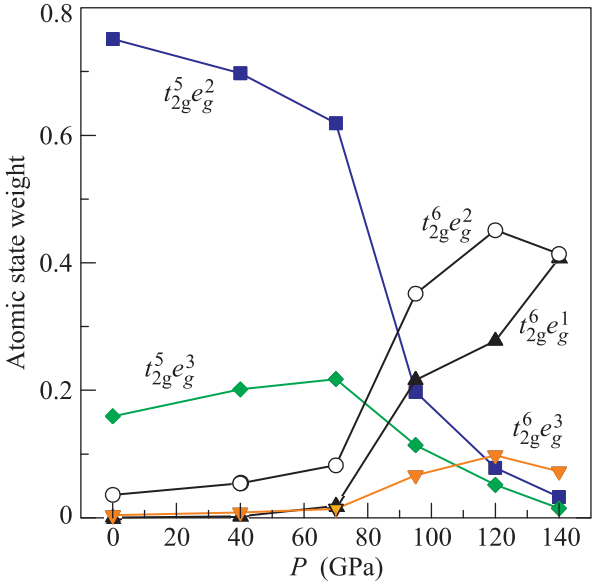

Fig. 6. Atomic state probabilities of Co-3d states versus pressure obtained in the LDA+DMFT calculations

weights characterize probabilities of particular atomic states. One can see that in CoO at AP the HS ($t_{2g}^5 e_g^2$) states prevail, however, starting from 80–95 GPa, contributions from the HS state (such as $t_{2g}^5 e_g^2$) decrease and system is characterized by a mixture of the low and intermediate spin configurations such as $t_{2g}^6 e_g^1$ and $t_{2g}^6 e_g^2$. Experimentally, these states might be difficult to distinguish especially taking into account structural rhombohedral distortions found at high pressure region [8, 9].

4. In conclusion. We have performed the LDA+DMFT calculations for CoO with the values of pressure from the ambient one till 140 GPa. In agreement with the experimental data the LDA+DMFT spectral functions of CoO at ambient pressure are characterized by a wide energy gap. At the pressures higher then 40 GPa, the spectral functions of CoO become metallic but only for the t_{2g} states while the e_g states remain insulating up to the very high pressures. This behavior corresponds to the orbital selective Mott transition scenario. The MIT obtained in our calculations is accompanied by the change of spin state which start to occur in CoO after 70 GPa. These results agree well with the high pressure x-ray emission spectroscopy and transport measurements.

The authors thank J. Kuneš for providing DMFT computer code used in our calculations, P. Werner for the CT–QMC impurity solver. Some libraries of the ALPS Project were used during the calculations [27]. This work was supported by the Russian Foundation for Basic Research (Projects # 10-02-00046 and 10-02-00546). A.V.L. acknowledges the support of MK-3376.2011.2.

1. M. Imada, A. Fujimori, and Y. Tokura, Rev. Mod. Phys. **70**, 1039 (1998).
2. J. Kuneš, A. V. Lukoyanov, V. I. Anisimov et al., Nature Materials **7**, 198 (2008).
3. J. Kuneš, Dm. M. Korotin, M. A. Korotin et al., Phys. Rev. Lett. **102**, 146402 (2009).
4. A. O. Shorikov, Z. V. Pchelkina, V. I. Anisimov, and S. L. Skornyakov, Phys. Rev. B **82**, 195101 (2010).
5. K. Held, I. A. Nekrasov, G. Keller et al., Phys. Stat. Sol. (b) **243**, 2599 (2006).
6. T. Atou, M. Kawasaki, and S. Nakajima, Jpn. J. Appl. Phys. **43**, L1281 (2004).
7. J.-P. Rueff, A. Mattila, J. Badro et al., J. Phys.: Condens. Matter **17**, S717 (2005).
8. K. Tomiyasu, T. Inami, and N. Ikeda, Phys. Rev. B **70**, 184411 (2004).
9. W. Jauch, M. Reehius, H. J. Bleifet al., Phys. Rev. B **64**, 052102 (2001).
10. Y. Noguchi, T. Atou, T. Kondo et al., Jpn. J. Appl. Phys. **38**, L7 (1999).
11. Q. Guo, H.-K. Mao, J. Hu et al., J. Phys.: Condens. Matter **14**, 11369 (2002).
12. K. Terakura, T. Oguchi, A. R. Williams, and J. Kübler, Phys. Rev. B **30**, 4734 (1984).
13. J. van Elp, J. L. Wieland, H. Eskes et al., Phys. Rev. B **44**, 6090 (1991).
14. R. E. Cohen, I. I. Mazin, and D. G. Isaak, Science **275**, 654 (1997).
15. V. I. Anisimov, J. Zaanen, and O. K. Anderson, Phys. Rev. B **44**, 943 (1991).
16. W. Zhang, K. Koepernik, M. Richter, and H. Eschrig, Phys. Rev. B **79**, 155123 (2009).
17. P. Giannozzi, S. Baroni, N. Bonini et al., J. Phys.: Condens. Matter **21**, 395502 (2009).

18. We used the pseudopotentials Co.pz-nd-rrkjus.UPF and O.pz-rrkjus.UPF from http://www.quantum-espresso.org.
19. G. H. Wannier, Phys. Rev. **52**, 191 (1937).
20. N. Marzari and D. Vanderbilt, Phys. Rev. B **56**, 12847 (1997).
21. Dm. Korotin, A. V. Kozhevnikov, S. L. Skornyakov et al., Eur. Phys. J. B **65**, 91 (2008).
22. A. I. Liechtenstein, V. I. Anisimov, and J. Zaanen, Phys. Rev. B **52**, R5467 (1995).
23. V. I. Anisimov and O. Gunnarsson, Phys. Rev. B **43**, 7570 (1991).
24. P. Werner, A. Comanac, L. de'Medici et al., Phys. Rev. Lett. **97**, 076405 (2006).
25. M. Jarrell and J. E. Gubernatis, Phys. Rep. **269**, 133 (1996).
26. V. I. Anisimov, I. A. Nekrasov, D. E. Kondakov et al., Eur. Phys. J. B **25**, 191 (2002).
27. http://alps.comp-phys.org; A. F. Albuquerque, F. Alet, P. Corboz et al., J. Magn. Magn. Mater. **310**, 1187 (2007); B. Bauer, L. D. Carr, H. G. Evertz et al., J. Stat. Mech. P05001 (2011).